Virus Detection

Quantitative Assessment of the Physical Virus Titer and Purity by Ultrasensitive Flow Virometry

Qian Niu[+], Ling Ma[+], Shaobin Zhu, Lan Li, Qisheng Zheng, Jibo Hou, Hong Lian, Lina Wu, and Xiaomei Yan*

Abstract: Rapid quantification of viruses is vital for basic research on viral diseases as well as biomedical application of virus-based products. Here, we report the development of a high-throughput single-particle method to enumerate intact viral particles by ultrasensitive flow virometry, which detects single viruses as small as 27 nm in diameter. The nucleic acid dye SYTO 82 was used to stain the viral (or vector) genome, and a laboratory-built nano-flow cytometer (nFCM) was employed to simultaneously detect the side-scatter and fluorescence signals of individual viral particles. Using the bacteriophage T7 as a model system, intact virions were completely discriminated from empty capsids and naked viral genomes. Successful measurement of the physical virus titer and purity was demonstrated for recombinant adenoviruses, which could be used for gene delivery, therapeutic products derived from phage cocktails, and infected cell supernatants for veterinary vaccine production.

The coronavirus disease-19 (COVID-19) pandemic caused by severe acute respiratory syndrome coronavirus 2 (SARS-CoV-2) has affected more than 96 million people globally since December 2019.[1–3] While viral infections remain a leading cause of morbidity and mortality worldwide, virus-based products are being developed for a diverse range of biomedical applications.[4–6] For example, vaccines based on inactivated or attenuated viruses are the first line of defense against infectious diseases.[7,8] Recombinant adenoviruses, adeno-associated viruses, lentiviruses, and other viruses are extensively used as vectors for gene therapy.[9,10] Oncolytic viruses, which have the ability to specifically infect and kill cancer cells, are used as cancer therapeutic agents.[11] Moreover, bacteriophages are being employed to combat antibiotic-resistant bacteria and as biocontrol agents in the food industry and animal husbandry.[12] Additionally, both the exterior and interior surfaces of virus-based nanoparticles can be engineered via chemical or genetic modification to display immunogenicity,[13] target specific cells,[14] and deliver therapeutic payloads.[15]

Viral titer measurement has always been a primary requirement as well as a laborious chore and a challenging task in virology. Given that a large number of impurities, such as cellular debris, incomplete or aberrant forms of virus particles, aggregates of bovine serum albumin, and free nucleic acids coexist with the complete mature virions in virus preparations, determining the true viral titer is among the most important quality control measures to ensure viral efficacy and potency.[16,17] The plaque assay is the classical method used for virus quantification, yet it requires 1–2 weeks (for mammalian viruses) or 1–2 days (for bacteriophages) to determine the infectious titers. Although the enzyme-linked immunosorbent assay (ELISA) and quantitative polymerase chain reaction (qPCR) can measure specific proteins and the nucleic acid sequences of viruses, respectively, the stringency of these "bulk" analytical methods is low, as they are incapable of distinguishing proteins originating from complete virions or empty capsids or soluble viral proteins and viral nucleic acids packed inside the capsid or that are free in solution.[18,19] Although new and elaborate methods are continuously developed for virus detection, very few of them are suitable for routine usage in virology research or quality control of viral products.[20–22]

With advancements in instrumentation, fluorescent dyes, and labeling strategies, flow cytometry, which has been commonly used for single cell analysis, has been used to analyze single viral particles, which was recently dubbed "flow virometry".[18,21,23–26] However, owing to the small size of viruses (17–350 nm, with the majority near or smaller than 100 nm) and the exponential dependence of the scattering intensity on particle size, elastically scattered light from single viruses usually falls below the limits of detection of the instruments and results in an under-counting of virus concentration.[27] Although great efforts have been made with regard to single virus detection on commercial instruments and custom-built instruments, it has been difficult to detect viruses smaller than 100 nm by light scattering measurements.[26,28,29] Therefore, nucleic acid staining is often implemented to discriminate viruses from the typical nonfluorescent background noise.[18,24,26] Nonetheless, concurrent detection of

[*] Q. Niu,[+] Dr. L. Ma,[+] Dr. S. Zhu, Dr. H. Lian, Dr. L. Wu,
Prof. Dr. X. Yan
Department of Chemical Biology, MOE Key Laboratory of Spectro-chemical Analysis & Instrumentation, Key Laboratory for Chemical Biology of Fujian Province, College of Chemistry and Chemical Engineering, Xiamen University
Xiamen 361005 (P. R. China)
E-mail: xmyan@xmu.edu.cn

L. Li, Dr. Q. Zheng, Dr. J. Hou
National Research Center of Engineering and Technology for Veterinary Biologicals, Jiangsu Academy of Agricultural Sciences
Nanjing 210014 (P. R. China)

Dr. J. Hou
Jiangsu Co-innovation Center for the Prevention and Control of Important Animal Infectious Diseases and Zoonoses
Yangzhou 225009 (P. R. China)

[+] These authors contributed equally to this work.

Supporting information and the ORCID identification number(s) for the author(s) of this article can be found under:
https://doi.org/10.1002/anie.202100872.

scattered light from single vial particles is important to discriminate complete virions from other noninfectious contaminants in viral preparations.[21] By integrating strategies for single-molecule fluorescence detection in a sheathed flow with approaches for reducing background scattering of cuvette windows and sheath fluid from reaching the detector, we constructed a nano-flow cytometer (nFCM) that enables light scattering detection of single silica nanoparticles and viruses as small as 24 and 27 nm in diameter, respectively.[30,31] For nFCM, the resolution for nanoparticle sizing is comparable to that of electron microscopy, and the size range covers the vast majority of viruses. Compared to conventional FCM, the significantly enhanced sensitivity of nFCM is based on a combined effect of 1) a reduced probe volume (ca. 25 fL) for background reduction, 2) an extended dwell time of the nanoparticles in the laser beam (0.3-2 ms) for increased photon generation, 3) a single-photon-counting avalanche photodiode (APD) detector for enhanced quantum efficiency of photon detection, and 4) an excellent optics to restrict the field-of-view of the APD detector solely to the sample stream for very good background rejection.[30,32] Taking advantage of the superior sensitivity of nFCM in both the side scatter and fluorescence detection of single nanoscale particles, here we report the development of a simple and rapid method to quantify the physical virus titer and purity. SYTO 82 nucleic acid stain was used for the first time to effectively label nucleic acids of all kinds of viruses including DNA, RNA, enveloped, and non-enveloped viruses without fixing or heating treatment.

Using the bacteriophage T7 (with an icosahedral capsid head of ca. 55 nm diameter and a genome DNA length of 39,937 bp)[33] as a model system, Figure 1a shows the schematic diagram of using the laboratory-built nFCM for the simultaneous detection of the side scatter (SSC) and fluorescence (FL) of single viruses. Membrane-permeable SYTO 82 was used to label the virus for 10 min owing to its good signal
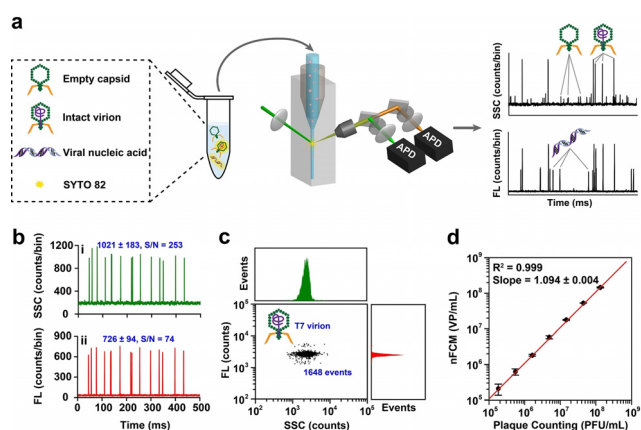
and excellent sample penetrance. The fluorescence excitation and emission maxima of DNA-bound SYTO 82 are 541 nm and 560 nm, respectively (Supporting Information, Figure S1). Intact virions, empty capsids, and free viral nucleic acids are expected to exhibit different features of SSC and FL signals. Figure 1b shows the representative burst traces of SSC (i) and FL (ii) signals in a 500-ms segment for a purified sample of the bacteriophage T7 (ca. 5.3×10^7 PFU mL^{-1}) stained with 1 µM SYTO 82. Owing to the superior sensitivity of the nFCM, for each individual T7 virion, the scattered light and fluorescence signals were detected concurrently with signal-to-noise (S/N) ratios of 253 and 74, respectively. After 1 minute of data acquisition, the bivariate dot-plot of the FL burst area versus the SSC burst area is shown in Figure 1c along with the burst area distribution histograms of SSC and FL. Fluorescent polystyrene beads 100 nm in diameter with known concentration were employed as an external standard to determine the concentration of virus particles (VP mL^{-1}) (Supporting Information, Figure S2).

The bacteriophage T7 was tested at a concentration ranging from 1.8×10^5 to 1.3×10^8 PFU mL^{-1}, and the linear correlation between the nFCM analysis and the plaque count was acquired with an R^2 of 0.999 and a slope of 1.094 ± 0.004. As shown in Table 1, reliable enumeration of bacteriophage

Table 1: Enumeration of bacteriophage T7 on the nFCM.

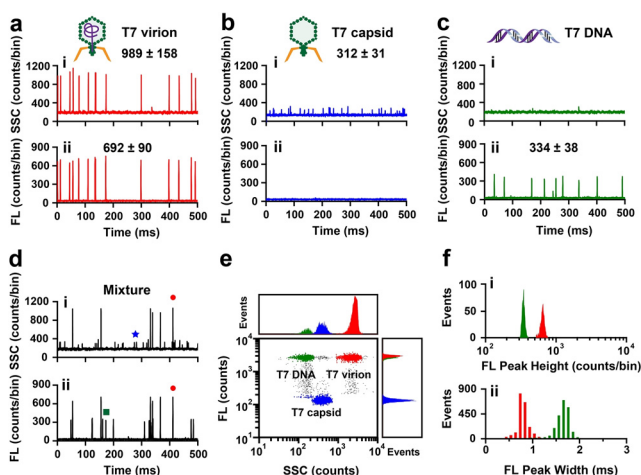| Plaque assay (PFU mL^{-1})	Event rate (particles min^{-1})	nFCM (VP mL^{-1})	VP-to-PFU ratio[a]
1.33×10^8	4488 ± 159	$(1.45 \pm 0.05) \times 10^8$	1.09
4.43×10^7	1644 ± 11	$(5.29 \pm 0.04) \times 10^7$	1.19
1.48×10^7	553 ± 16	$(1.78 \pm 0.05) \times 10^7$	1.20
4.93×10^6	183 ± 18	$(5.91 \pm 0.59) \times 10^7$	1.20
1.64×10^6	57 ± 4	$(1.84 \pm 0.11) \times 10^6$	1.12
5.47×10^5	20 ± 4	$(6.33 \pm 1.27) \times 10^5$	1.16
1.82×10^5	7 ± 2	$(2.11 \pm 0.73) \times 10^5$	1.16

[a] VP-to-PFU ratio is defined as the number of virus particles (VP) measured by nFCM enumeration divided by the number of plaque forming units (PFU) obtained by the traditional viral plaque assay.

T7 can be attained at a concentration as low as 2×10^5 VP mL^{-1} with 1 min of data acquisition. If the data acquisition time is extended to 10 min or more, accurate counting should be obtained for a concentration of 2×10^4 VP mL^{-1} or lower. This limit of detection (LOD) is certainly inferior to the 1–10 viruses for the plaque assay or qPCR-based techniques. Yet, the nFCM enumeration can be accomplished in less than 30 minutes and can eliminate the interference of viral nucleic acids in solution. Thus nFCM is far more efficient and practical for the routine quality control of viral products, of which the virus concentration is normally higher than 10^6 VP mL^{-1}.[34–36]

Robust discrimination between intact viruses and virus-like particles is the prerequisite for the effective quantification of the virus titer. To examine the feasibility of using nFCM to differentiate intact virions, empty capsids, and viral genomes in a mixture, these three constituents were first analyzed separately after staining with 1 µM SYTO 82. Similar to Figure 1b, Figure 2a indicates that both the SSC

Figure 1. a) Diagram of the laboratory-built nFCM for the simultaneous detection of the side scatter (SSC) and fluorescence (FL) of single viruses. b),c) Representative SSC and FL burst traces (b) and the bivariate dot-plot of FL versus SSC derived from data collected over 1 min (c) for the bacteriophage T7 stained by 1 µM SYTO 82. d) Linear relationship between the concentrations of the bacteriophage T7 measured by nFCM enumeration and the traditional plaque assay; data are represented as the mean ± SD (*n* = 3).

Figure 2. Differentiation of intact virions, empty capsids, and free viral DNA by nFCM. a)–d) Typical SSC and FL burst traces for T7 virions (a), empty T7 capsids (b), T7 DNA molecules (c), and a mixture of these three constituents (d). e) A bivariate dot-plot of FL versus SSC for the mixture from data collected over 1 min. f) Fluorescence peak-height-distribution (i) and peak-width-distribution (ii) histograms for virus-encapsulated T7 DNA and free T7 DNA molecules in the mixture.

and FL signals of intact T7 virions were detected with excellent sensitivity. For the T7 empty capsid, only the SSC signal was detected, and the amplitude (312 ± 31 counts/bin) (Figure 2b) was much lower than that of the intact T7 virion (989 ± 158 counts/bin). This can be attributed to the lower refractive index of the empty capsid compared to that of the intact virion, which thus scatters less laser light.[37] Figure 2c reveals that T7 DNA that was free in solution exhibited only FL signals, and no concurrent scattered light was detected. However, to our surprise, the FL peak height (334 ± 38 counts/bin) was only approximately 48% of that obtained for the intact T7 virion (692 ± 90 counts/bin), which was inconsistent with the equal length of the nucleic acids. We then mixed these three constituents and analyzed them by nFCM. Figure 2d shows the typical burst traces of the SSC and FL signals, in which a representative intact virion, empty capsid, and viral DNA from T7 are marked by a red circle ●, blue star ★, and green square ■, respectively. The bivariate dot-plot of FL versus SSC indicates that T7 capsids and T7 DNA can clearly be resolved from T7 virions (Figure 2e). Interestingly, the fluorescence intensities of virus-containing DNA molecules and free T7 DNA are approximately the same despite their largely different fluorescence peak heights (Figures 2a(ii) and 2c(ii)). This phenomenon can be explained by comparing the peak height and peak width of these two constituents (Figure 2f, i and ii). Virus-encapsulated DNA exhibits a relatively high peak intensity and short pulse duration compared with viral DNA free in solution, which passes through the measurement probe volume in an extended conformation owing to stretching by the hydrodynamic forces that arise where the sample enters the flow cell,[38] which results in a lower peak signal but a longer pulse duration. The distinct discrimination of individual virions from empty viral capsids and free viral DNA suggests the

great potential of nFCM for the characterization of the entrapment efficiency of virus-based gene-delivery systems.

Viruses have evolved specialized molecular mechanisms to efficiently transport their genomes inside the cells they infect and thus can serve as nanoscale vehicles for the delivery of nucleic-acid cargos into host cells.[9] For example, vectors of adenovirus (Ad), a nonenveloped virus with an 80–120 nm icosahedral protein capsid containing a dsDNA genome of approximately 36,000 bp, have been extensively studied in experimental and clinical models of gene delivery.[39] During the production of recombinant Ad (rAd), empty capsids and incompletely processed viral proteins always coexist with mature virions (Figure 3a). Thus, the efficacy of gene transfer
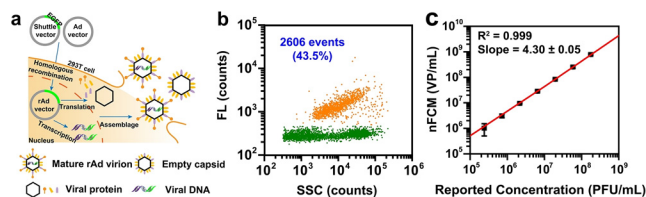

Figure 3. Characterization of the commercial rAd-EGFP vector. a) Depiction of the production process of the rAd-EGFP vector. b) Bivariate dot-plot of FL versus SSC for a 1620-fold diluent of commercial rAd-EGFP vector from data collected over 1 min. c) Linear correlation between the concentration of complete rAds measured by nFCM enumeration and the concentration of infectious virions reported by the manufacturer; data are represented as the mean ± SD ($n=3$).

will be significantly influenced by the percentage of infectious particles in a given viral vector stock. Figure 3b and 3c shows the nFCM analysis of a commercial rAd-EGFP vector that was developed for neural tracing by delivering a green fluorescent protein gene to neurons. To minimize the enhanced fluorescence background caused by free DNA, a 810-fold dilution of the commercial rAd-EGFP vector was treated with DNase I ($1.4 \text{ U } \mu\text{L}^{-1}$, 37°C for 30 min) prior to staining with 1 μM SYTO 82 via 1:1 volume mixing with 2 μM SYTO 82 solution. We can see from the bivirate dot-plot of FL versus SSC that mature rAd-GFP virions (orange dots) can be easily differentiated from impurities (green dots) upon nucleic acid staining, and the purity of the rAd-EGFP sample (defined as the events of mature virions divided by the total events measured by side scatter) was 43.5% (Figure 3b). It is worth noting that extracellular vesicles secreted by host cells may contribute to the total particle counts, as they are common contaminants of viral preparations.[18,21] Compared with the manufacturer's reported concentration ($3.16 \times 10^{10} \text{ PFU mL}^{-1}$), the concentration of mature rAd-EGFP virion measured by nFCM via single-particle enumeration was ca. 4.33-fold higher ($1.37 \times 10^{11} \text{ particles mL}^{-1}$). These findings indicate that a certain percentage of complete virions are defective. For rAd-EGFP diluted with different factors, a good linear correlation between the complete virion concentrations measured by the nFCM and the PFU concentration provided by the manufacturer was obtained with an R^2 of 0.999 (Figure 3c).

As bacterial predators, bacteriophages are considered valuable antimicrobial agents in the food industry and animal husbandry.[40] The advantages of bacteriophages over anti-biotics include great specificity to host bacteria that reduces damage caused to the normal host microbiota and lower propensity to induce resistance, especially when using a phage cocktail. Figure 4 shows the phage concentration measure-
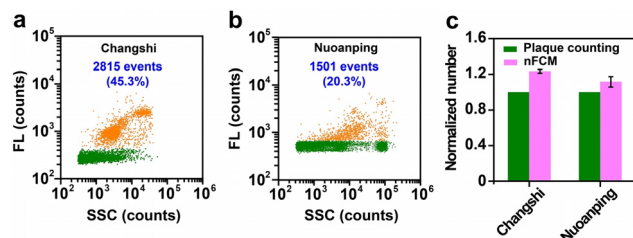
Figure 4. Virus concentration measurement of two commercial phage cocktail products. a),b) Bivariate dot plots of FL versus SSC for 2000-fold diluent of Changshi (a) and 200-fold diluent of Nuoanping (b) from data collected over 1 min each. c) Comparison of phage concentrations obtained by plate counting and nFCM; data are represented as the mean $\pm$ SD ($n = 3$).

ments of two commercial phage products by nFCM. The phage cocktail Changshi contains seven different phages (Supporting Information, Table S1) and is used to kill pathogenic *Escherichia coli* and *Salmonella* in the intestines of poultry without harmful effects on probiotic bacteria. Upon DNase I treatment and SYTO 82 staining, Figure 4a shows the bivariate dot-plot of SYTO 82 fluorescence versus SSC for a 2000-fold diluent of Changshi, and 2815 events with concurrent SSC and FL signals were detected in 1 minute. The original concentration of intact phages in the Changshi cocktail was measured to be 1.81×10^{11} particles mL^{-1}. Phage cocktail Nuoanping is another commercial product that contains two different phages and is used to treat *Staphylococcus aureus* infections in poultry and livestock. Owing to its slightly lower particle concentration compared to Changshi, it was diluted 100-fold, treated with DNase I, stained with SYTO 82, and analyzed by nFCM. We can see from the bivariate dot-plot shown in Figure 4b that the signal of intact virions in Nuoanping was quite diverse, and the original phage concentration was determined to be 9.65×10^9 particles mL^{-1}. We also noticed that due to the 10-fold lower dilution than Changshi, the fluorescence background of the Nuoanping diluent was slightly higher owing to the existence of a large amount of DNA molecules in the product. Our results clearly indicate that a large number of

impurity components exist in the final products of phage cocktails. Thus, quantification of physical virus titers and impurity particles is critical to the potency of phage-based products. Compared with the plate counting results (1.47×10^{11} PFU mL^{-1} for Changshi and 8.25×10^9 PFU mL^{-1} for Nuoanping) reported by the manufacturers, the virion count measured by nFCM was slightly higher with VP-to-PFU ratios of 1.2 and 1.1, respectively (Figure 4c). These results again revealed that some intact virions are noninfectious.

Inactivated viruses are widely used as both human and veterinary vaccines. As viral stocks harvested from cell culture media typically contain a mixture of defective and infectious particles, rapid and reliable quantification of intact virus particles is valuable for the timely support of upstream process development.[21] To evaluate the capability of the as-developed method in characterizing both the DNA and RNA viruses, infected cell supernatants for veterinary vaccine production of porcine epidemic diarrhea virus (PEDV, an enveloped coronavirus with a 120 nm protein capsid containing a linear ssRNA genome of 28 kb) and pseudorabies virus (PRV, an enveloped herpesvirus with a 150–200 nm protein capsid containing a linear dsDNA genome of 150 kb) were analyzed. As illustrated in Figure 5a, the main steps of producing virus-based vaccines include virus inoculation, harvest, purification, and emulsification. Here, virus preparations #A, #B, and #C are used to denote the products obtained upon harvest and after the first and second purification steps, respectively. Figure 5b indicates that for preparation #A of the PEDV vaccine, 1227 events with concurrent SSC and FL signals were detected in 1 min of data acquisition. The corresponding concentration of complete virions was determined to be 4.0×10^9 particles mL^{-1}, and the purity of intact viruses was 20.4 %. Figure 5c shows the result for virus preparation #A of the PRV vaccine; 1026 fluorescent particles were detected in 1 minute, and the concentration of intact virus was determined to be 3.3×10^9 particles mL^{-1}.
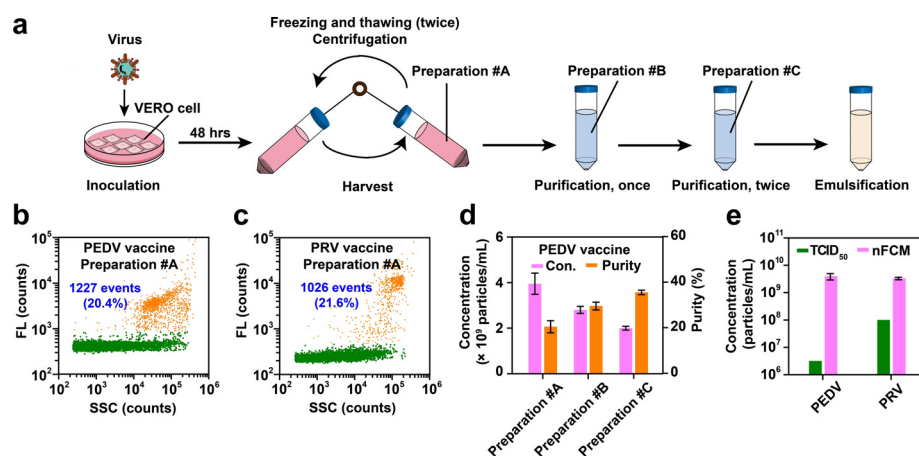
Figure 5. Characterization of virus-based vaccines by nFCM. a) Depiction of the main production steps for virus-based vaccines. b) Bivariate dot-plot of FL versus SSC for preparation #A of the PEDV vaccine. c) Bivariate dot-plot of FL versus SSC for preparation #A of the PRV vaccine. d) Viral concentration and purity of complete virions upon harvest, first purification, and second purification of the PEDV vaccine. e) Comparison between the virus concentration of PEDV and PRV measured by the TCID$_{50}$ assay and nFCM method; data are represented as the mean $\pm$ SD ($n = 3$). The dilution factor of the samples was 100, and the data acquisition time was 1 min for each sample.

9354 www.angewandte.org

© 2021 Wiley-VCH GmbH

Angew. Chem. Int. Ed. **2021**, 60, 9351 –9356

Figure 5d indicates that further purification upon precipitation results in a decrease in the intact virus concentration along with an increase in purity. Compared with the classic SDS-PAGE assay used to detect impurities, nFCM is much faster and quantitative in terms of assessing the purity of viral products. The concentrations of virus particles in preparation #A of both vaccines were also measured by the 50% tissue culture infective dose assay ($TCID_{50}$), and their comparison with the results determined by nFCM is plotted in Figure 5e. Clearly, the virus concentration measured by $TCID_{50}$ was 1–3 orders of magnitude lower than that determined by nFCM. The relatively low infectivity of intact virions has been reported for mammalian viruses, which could be attributed to the expression of nonfunctional envelope proteins on the surface of viruses.[18,26]

To further examine the accuracy of nFCM in virus quantification, qPCR assay was conducted for rAD-EGFP vector and RPV vaccine. Virus titers measured by plaque assay, nFCM, and qPCR are listed in Table 2 and Table S3 for comparison. These results highlight the presence of intact but non-infective virions and the abundant presence of naked viral nucleic acids in viral vector and vaccine preparations. In

Table 2: Comparison of virus titers measured by plaque assay, nFCM, and qPCR.

	Plaque assay ($IU\,mL^{-1}$)[a]	nFCM ($VP\,mL^{-1}$)	VP-to-IU ratio	qPCR ($genome\,mL^{-1}$)	Genome-to-IU ratio
rAd-EGFP	3.16×10^{10}	$(1.37 \pm 0.03) \times 10^{11}$	4.33 ± 0.08	$(2.55 \pm 0.01) \times 10^{12}$	80.70 ± 0.18
PRV	1.00×10^{8}	$(3.30 \pm 0.07) \times 10^{9}$	33.03 ± 0.69	$(1.86 \pm 0.03) \times 10^{10}$	186.45 ± 2.83

[a] IU refers to infectious unit. The manufacturers reported IUs were $PFU\,mL^{-1}$ for rAd-EGFP vector and $TCID_{50}\,mL^{-1}$ for PRV vaccine, respectively.

particular, physical virus titers measured by nFCM agreed much better with the infectious units determined by plaque assay than the viral genome titers quantified by qPCR. It is worth noting that for vaccines based on inactivated viruses, it is the intact virions that play the role of antigen, and there is no requirement for whether the virus is infectious or not before inactivation. Therefore, the physical virus titer measured by nFCM is more meaningful for vaccine preparations than the infection titer measured by plaque assay.

In summary, based on the superior sensitivity and through concurrent detection of individual viral entities via light scatter and fluorescence in a high-throughput manner, nFCM provides a powerful approach to detect all kinds of viruses, including DNA, RNA, enveloped, and non-enveloped viruses during process development and production. Thus, the nFCM-based assay can serve as a simple, rapid, and accurate method for the routine use in quality control of virus preparations, such as viral vaccines, viral vectors, and phage cocktails. In addition to nucleic acid staining, nFCM could be directly applicable to the analysis of genetically modified viruses expressing fluorescently tagged virion components, viruses labeled with antibodies, or enveloped viruses labeled with lipid dyes. It could also be used to address new and unanswered questions about individual virus heterogeneity with great statistical rigor.

Conflict of interest

X.Y. and S.Z. declare competing financial interest as cofounders of NanoFCM Inc., a company committed to commercializing the nano-flow cytometry (nFCM) technology. L.M. declares competing financial interests as shareholder and employee of NanoFCM Inc.

[1] N. J. Matheson, P. J. Lehner, *Science* **2020**, *369*, 510–511.
[2] J. Shang, G. Ye, K. Shi, Y. Wan, C. Luo, H. Aihara, Q. Geng, A. Auerbach, F. Li, *Nature* **2020**, *581*, 221–224.
[3] N. Zhang, X. Li, Y. Deng, H. Zhao, Y. Huang, G. Yang, W. Huang, P. Gao, C. Zhou, R. Zhang, Y. Guo, S. Sun, H. Fan, S. Zu, Q. Chen, Q. He, T. Cao, X. Huang, H. Qiu, J. Nie, Y. Jiang, H. Yan, Q. Ye, X. Zhong, X. Xue, Z. Zha, D. Zhou, X. Yang, Y. Wang, B. Ying, C. Qin, *Cell* **2020**, *182*, 1271–1283.
[4] S. M. Jones, H. Feldmann, U. Ströher, J. B. Geisbert, L. Fernando, A. Grolla, H.-D. Klenk, N. J. Sullivan, V. E. Volchkov, E. A. Fritz, K. M. Daddario, L. E. Hensley, P. B. Jahrling, T. W. Geisbert, *Nat. Med.* **2005**, *11*, 786–790.
[5] R. Waehler, S. J. Russell, D. T. Curiel, *Nat. Rev. Genet.* **2007**, *8*, 573–587.
[6] H. Hu, H. Masarapu, Y. N. Gu, Y. F. Zhang, X. Yu, N. F. Steinmetz, *ACS Appl. Mater. Interfaces* **2019**, *11*, 18213–18223.
[7] S. Caddy, *Br. Med. J.* **2020**, *369*, 1–2.
[8] M. T. Osterholm, N. S. Kelley, A. Sommer, E. A. Belongia, *Lancet Infect. Dis.* **2012**, *12*, 36–44.
[9] M. A. Kotterman, D. V. Schaffer, *Nat. Rev. Genet.* **2014**, *15*, 445–451.
[10] K. Lundstrom, *Diseases* **2018**, *6*, 42–62.
[11] H. L. Kaufman, F. J. Kohlhapp, A. Zloza, *Nat. Rev. Drug Discovery* **2015**, *14*, 642–662.
[12] G. P. C. Salmond, P. C. Fineran, *Nat. Rev. Microbiol.* **2015**, *13*, 777–786.
[13] Y. Zhao, Z. Li, X. Zhu, Y. Cao, X. Chen, *Biomaterials* **2020**, *249*, 120030.
[14] G. J. Tong, S. C. Hsiao, Z. M. Carrico, M. B. Francis, *J. Am. Chem. Soc.* **2009**, *131*, 11174–11178.
[15] N. Stephanopoulos, G. J. Tong, S. C. Hsiao, M. B. Francis, *ACS Nano* **2010**, *4*, 6014–6020.
[16] B. Metz, G. van den Dobbelsteen, C. van Els, J. van der Gun, L. Levels, L. van der Pol, N. Rots, G. Kersten, *Expert Rev. Vaccines* **2009**, *8*, 227–238.
[17] K. Gao, M. X. Li, L. Zhong, Q. Su, J. Li, S. Y. Li, R. He, Y. Zhang, G. Hendricks, J. Z. Wang, G. P. Gao, *Mol. Ther. Methods Clin. Dev.* **2014**, DOI: https://doi.org/10.1038/mtm.2013.9.
[18] T. M. Renner, V. A. Tang, D. Burger, M. A. Langlois, *J. Virol.* **2020**, *94*, e01600–e01619.
[19] S. Heider, C. Metzner, *Virology* **2014**, *462*, 199–206.

[20] N. Boonham, J. Kreuze, S. Winter, R. van der Vlugt, J. Berger-voet, J. Tomlinson, R. Mumford, *Virus Res.* **2014**, *186*, 20–31.

[21] J. L. R. Zamora, H. C. Aguilar, *Methods* **2018**, *134*, 87–97.

[22] L. Yang, T. Yamamoto, *Front. Microbiol.* **2016**, *7*, 1500.

[23] A. Arakelyan, W. Fitzgerald, L. Margolis, J. C. Grivel, *J. Clin. Invest.* **2013**, *123*, 3716–3727.

[24] R. Gaudin, N. S. Barteneva, *Nat. Commun.* **2015**, *6*, 6022–7022.

[25] S. Zicari, A. Arakelyan, W. Fitzgerald, E. Zaitseva, L. V. Chernomordik, L. Margolis, J. C. Grivel, *Virology* **2016**, *488*, 20–27.

[26] R. Lippe, *J. Virol.* **2018**, *92*, 1–11.

[27] I. González-Domínguez, E. Puente-Massaguer, L. Cervera, F. Godia, *Viruses* **2020**, *12*, 1–24.

[28] M. Hercher, W. Mueller, H. M. Shapiro, *J. Histochem. Cytochem.* **1979**, *27*, 350–352.

[29] H. B. Steen, *Cytometry Part A* **2004**, *57*, 94–99.

[30] S. Zhu, L. Ma, S. Wang, C. Chen, W. Zhang, L. Yang, W. Hang, J. P. Nolan, L. Wu, X. Yan, *ACS Nano* **2014**, *8*, 10998–11006.

[31] L. Ma, S. Zhu, Y. Tian, W. Zhang, S. Wang, C. Chen, L. Wu, X. Yan, *Angew. Chem. Int. Ed.* **2016**, *55*, 10239–10243; *Angew. Chem.* **2016**, *128*, 10395–10399.

[32] H. Lian, S. B. He, C. X. Chen, X. M. Yan, *Annu. Rev. Anal. Chem.* **2019**, *12*, 389–409.

[33] M. E. Cerritelli, N. Q. Cheng, A. H. Rosenberg, C. E. McPherson, F. P. Booy, A. C. Steven, *Cell* **1997**, *91*, 271–280.

[34] G. Tiscornia, O. Singer, I. M. Verma, *Nat. Protoc.* **2006**, *1*, 241–245.

[35] P. Jault, T. Leclerc, S. Jennes, J. P. Pirnay, Y. A. Que, G. Resch, A. F. Rousseau, F. Ravat, H. Carsin, R. Le Floch, J. V. Schaal, C. Soler, C. Fevre, I. Arnaud, L. Bretaudeau, J. Gabard, *Lancet Infect. Dis.* **2019**, *19*, 35–45.

[36] A. Jorritsma-Smit, C. J. van Zanten, J. Schoemaker, J. J. M. Meulenberg, D. J. Touw, J. G. W. Kosterink, H. W. Nijman, T. Daemen, D. P. Allersma, *Eur. J. Pharm. Sci.* **2020**, *143*, 105096–105104.

[37] L. Fumagalli, D. Esteban-Ferrer, A. Cuervo, J. L. Carrascosa, G. Gomila, *Nat. Mater.* **2012**, *11*, 808–816.

[38] R. C. Habbersett, J. H. Jett, *Cytometry Part A* **2004**, *60*, 125–134.

[39] B. L. Davidson, X. O. Breakefield, *Nat. Rev. Neurosci.* **2003**, *4*, 353–364.

[40] C. Carvalho, A. R. Costa, F. Silva, A. Oliveira, *Crit. Rev. Microbiol.* **2017**, *43*, 583–601.